Available online at www.sciencedirect.com

ScienceDirect

Procedia Engineering 98 (2014) 28 – 35

Procedia Engineering

www.elsevier.com/locate/procedia

11th International Symposium on Systems with Fast Ionic Transport, ISSFIT 11

Highly conductive $90V_2O_5 \cdot 10P_2O_5$ nanocrystalline cathode materials for lithium-ion batteries

Tomasz K. Pietrzak*, Łukasz Pawliszak, Przemysław P. Michalski, Marek Wasiucionek, and Jerzy E. Garbarczyk

Faculty of Physics, Warsaw University of Technology, Koszykowa 75, 00-662 Warsaw, Poland

Abstract

The aim of this research was to optimize process of nanocrystallization of vanadate-phosphate glasses in order to reach as high electronic conductivity as possible. $90V_2O_5 \cdot 10P_2O_5$ glasses were prepared by a standard melt-quenching technique under different synthesis conditions. The glass transition temperature, the crystallization temperature and the electric conductivity at RT is evidently correlated with the synthesis temperature. The samples were annealed at different temperatures. As a result of this optimization, a sample with $\sigma(25\ °C) = 0.7 \cdot 10^{-1}$ S/cm was synthesized. The microstructure of the sample consists of V_2O_5 nanocrystallites with size within 15÷30 nm. The significant increase in the conductivity is discussed in terms of the Mott's model of electron hopping and a core-shell concept. The electrochemical measurements have shown that up to 3 moles of Li^+ ions can be inserted into 1 mole of V_2O_5.

Peer-review under responsibility of the Gdansk University of Technology

Keywords: nanomaterials; nanocrystallization; V_2O_5; hopping conductivity; cathode materials; Li-ion batteries

1. Introduction

Vanadium oxides have since long time been interesting as alternative cathode materials for lithium and Li-ion batteries [1]. Recently Whittingham et al. used some vanadium oxides additives to improve electrical and

* Corresponding author. Tel.: +48 22 234 8674; fax: +48 22 628 21 71.
E-mail address: topie@if.pw.edu.pl

Peer-review under responsibility of the Gdansk University of Technology
doi:10.1016/j.proeng.2014.12.483

electrochemical properties of $LiFePO_4$ olivines [2,3]. Our recent studies have shown that olivine-like materials with addition of V_2O_5 exhibit relatively high electronic conductivity – 10^{-3} S/cm at room temperature [4]. One of ways to improve the properties of many solids is to prepare them as nanomaterials. This holds also for cathode materials for Li-ion batteries. Nanocrystalline nature of the active material leads to the enhanced ionic transport [5] and improved electrochemical performance [6]. Crystalline forms of vanadates have been investigated for decades and are well characterized. Much less is known about physical properties of their amorphous or nanostructural analogs [7,8]. In our recent papers we have reported that thermal nanocrystallization of vanadate-phosphate glasses leads to significant increase in their electronic conductivity and improved thermal stability [9, 10, 11]. Most of our studies have been focused on materials with nominal composition $90V_2O_5{\cdot}10P_2O_5$ [8,12]. The addition of P_2O_5, a supporting glass former, was necessary to prepare fully amorphous samples via a typical glass-making process like melt-quenching. Furthermore, our research on nanocrystalline V_2O_5 (prepared via a twin-roller technique) have shown that the conditions of the synthesis have a significant influence on electric and thermal properties of the samples [13]. Therefore, we decided to perform nanocrystallization of a series of $90V_2O_5{\cdot}10P_2O_5$ glasses obtained under different synthesis conditions, in order to reach as high electronic conductivity as possible.

2. Experimental

Amorphous samples of nominal composition $90V_2O_5{\cdot}10P_2O_5$ were prepared from commercial predried chemicals: V_2O_5 (ABCR, 99.5%) and $(NH_4)H_2PO_4$ (POCh – Polish Chemicals, 99.5%), which were ground and mixed in agate mortar and divided into 6 batches, labeled as P_1,... P_6. Alumina crucibles filled with the powders were placed in an electric furnace, heated in air to different temperatures within 800÷1300 °C range, and held at that temperature for 15÷60 min. The details of this procedure are presented in Table 1. Eventually, the molten mixtures were rapidly poured out onto a stainless-steel plate held at room temperature and immediately pressed with another identical plate. The average thickness of the resulting samples was ca. 0.7 mm. X-ray diffraction (XRD) patterns were collected using a Philips X'Pert Pro apparatus equipped with a copper anode and a Ni filter. The CuKα radiation of wavelength λ = 1.542 Å was used in the experiments. Diffraction patterns confirmed amorphousness of the as-prepared material and revealed information about the nanostructure of the samples after the thermal treatment. Thermal events occurring in the samples were observed with a TA DSC Q200 instrument. DSC scans were carried out in a non-isothermal mode from ca. 40 to 550 °C, at a series of heating rates (1 ÷ 40 °C/min). The electrical conductivity measurements were carried out by impedance spectroscopy. The setup was based on a Solartron 1260 Gain Phase/Impedance Analyzer integrated with an oven and modules for temperature programming and stabilization (Eurotherm 2404). The samples were heated from the room temperature up to a wide variety of temperatures and consequently cooled down to RT. Their electronic conductivity was measured in-situ during this heat-treatment, in order to observe the influence of the nanocrystallization on the electronic conductivity and to compare the electric results with the thermal analyses. SEM images of selected samples were taken in order to examine their microstructure.

Table 1. Details on the synthesis conditions of the samples.

Batch ID	P_1	P_2	P_3	P_4	P_5	P_6
Temperature / °C	800	950	1100	1100	1200	1300
Annealing time / min.	15	15	15	60	60	60

The batch with the highest electronic conductivity (P_6) was selected for electrochemical measurements. About 5 g of the powdered sample was heated to 450 °C in a tube furnace, with a thermal program similar to the one used in the electric measurements. Then the sample was ball-milled with a Retch PM100 planetary mill in order to prepare a cathode layer. Galvanostatic charge-discharge cycling tests were using an Autolab PGSTAT30. The cathode was prepared from the P_6 sample (70% wt active material, 20% wt carbon black (CB) and 10% wt PVDF). It was cut in disks of 12 mm in diameter with a loading of about 4 mg/cm^2 of active material. Metallic lithium plate was used as an anode. The cell was discharged with C/20 current without a voltage cut-off, until maximum theoretical capacity

was reached. This was to determine maximum amount of lithium that can be intercalated into the structure. The maximum theoretical capacity (Q_{max} = 398 mAh/g) was calculated, assuming that lithium ions can be intercalated only into V_2O_5 structure, but not P_2O_5.

3. Results

3.1. XRD

Powder diffraction patterns of as-received samples proved that they were fully amorphous. For low angles a wide halo, related to close order in glassy materials, was observed. No Bragg reflections are observed, except for a single tiny peak for batch P_6. The diffractogram of the sample P_6 heated up to 450 °C are typical for a nanocrystalline material. The broad XRD peaks were identified as of an orthorhombic V_2O_5 structure (JCPDS-ICDD card no. 00-041-1426). The grain size, as determined from the line broadening [14] varies from 15 to about 30 nm, depending on *hkl* indices. The average value of grain size equals 21 nm.

3.2. DSC

In DSC curves for all the as-received samples (Fig. 1) a discernible baseline shift (characteristic for a glass transition) was followed by an exothermic peak (crystallization). The temperatures of these transitions, T_g and T_c respectively, increased with an increasing temperature of synthesis in an approximately linear way (Fig. 2). It is commonly known that the temperatures of the thermal events in DSC experiments depend on the heating rate. This rule has been shown also in our recent papers [8, 12, 15]. A very simple empirical expression describing T_g vs. the heating rate, which even so has been rarely used (e.g. by [16]), was proposed earlier by M. Lasocka [17]:

$$T_g = A + B \ln \theta \tag{1}$$

where: A, B – empirical constants, θ – heating rate in °C/min. A practical advantage of this expression, except its simplicity, is that fitting parameter A equals the glass transition temperature upon heating with θ = 1 °C/min. Experimental data presented in appropriate coordinates show that Eq. 1 can be successfully applied to describe the T_g vs. θ in case of the glasses under study (Fig. 3). Furthermore, the slope of the fitted lines is comparable for all the as-received samples (with the exception of the sample P_2).

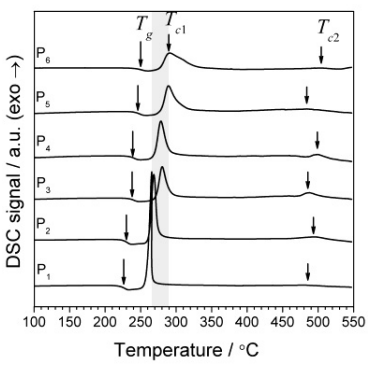

Fig. 1. DSC curves of the as-received glasses.

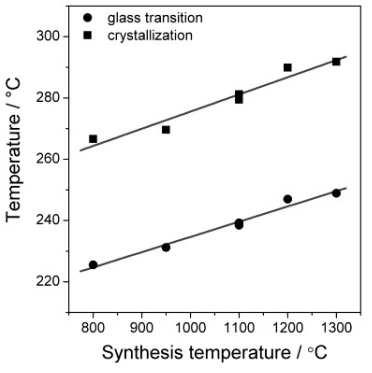

Fig. 2. Experimental dependencies of the glass transition and crystallization temperatures on the glass synthesis temperature.

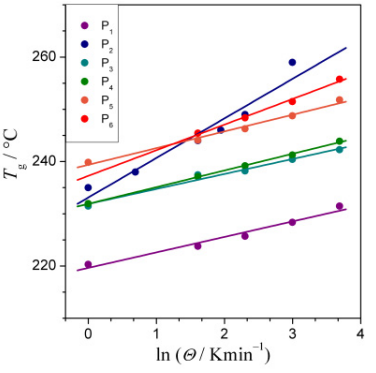

Fig. 3. The glass transition temperatures determined from DSC measurements vs. the heating rate θ.

Crystallization phenomena occurring during non-isothermal heating of glasses have been successfully represented by the Kissinger formula [18]:

$$\ln\left(\frac{\theta}{T_m^2}\right) = -\frac{Q}{k_B T} + C \tag{2}$$

where: θ – heating rate, T_m – temperature of maximum of the crystallization peak, k_B – Boltzmann constant, Q – activation energy of the crystallization process and C – a constant. In some cases, Kissinger formula may also be used to describe dependence of the glass transition temperature on the heating rate [19]. In case of glasses studied in this work, the Kissinger equation applies satisfactorily to both glass transition and crystallization phenomena. The values of the activation energies of the glass transition and the crystallization varies from 2.8 to 7.1 eV and from 1.66 to 3.02 eV, respectively.

3.3. Electronic conductivity

The conductivity of as-received glassy samples was measured at RT for several samples of each batch. The average values of the conductivity, which are between $2{\cdot}10^{-5}$ and $8{\cdot}10^{-5}$ S/cm, are presented in Fig. 4. One can see that the values of the electronic conductivity grow with the temperature of the synthesis and this dependence can be fitted with a straight line. As mentioned in the Experimental, each as-received material was heated to a certain maximum temperature and then cooled down to RT. The maximum temperature values varied from 300 to 550 °C. The relative increase in the conductivity at RT, represented by a ratio of its values before and after the thermal treatment, which is somewhere between one and three orders of magnitude, is shown in Fig. 5. In general, the most pronounced increase was observed for the sample P_6, previously synthesized at 1300 °C. Moreover, the ratio exhibited a sort of a plateau for moderate temperatures (ca. 400 °C) of the thermal treatment.

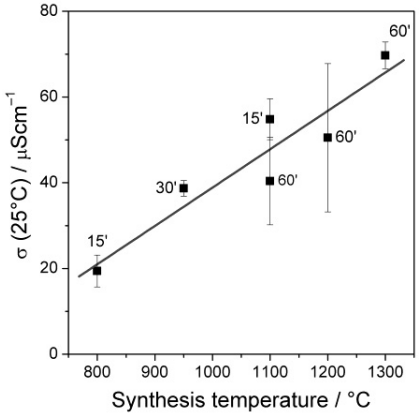

Fig. 4. Experimental dependence of room temperature electronic conductivity of the as-received samples (glasses) on synthesis temperature.

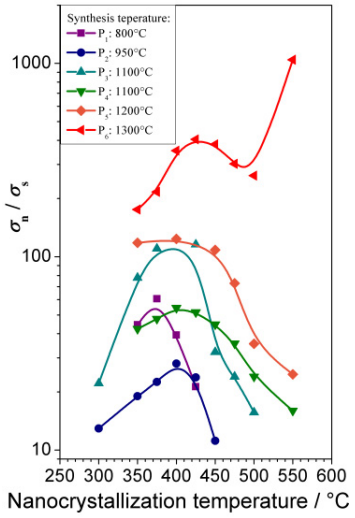

Fig. 5. Relative increase in the electronic conductivity (at 25°C) as a result of thermal nanocrystallization.

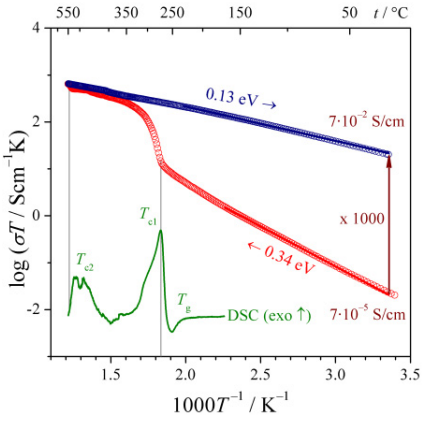

Fig. 6. Temperature dependence of the electronic conductivity of sample P_6 upon heating to 550°C (1°C/min.) and cooling down to RT.

The temperature dependence of the electronic conductivity follows the well-known Arrhenius formula. The temperature dependence of the electronic conductivity of the sample P_6 heated up to 550°C and cooled down is shown in Fig. 6. This thermal treatment resulted in the best-conducting sample with conductivity of 0.07 S/cm at 25°C. The significant increase in the conductivity is correlated with the crystallization process observed during the thermal analysis of the sample. It is worth noticing that the thermal treatment was repeated for several samples resulting in a very good reproducibility of the results. The reproducibility of the nanocrystallization described previously for small samples was checked for more massive sample of P_6 (ca. 5 g) in another tube furnace. The conductivity (at RT) and the activation energy of the sample annealed up to 450°C were $1.5 \cdot 10^{-2}$ S/cm and 0.19 eV, respectively – very similar to the sample annealed to the same temperature during impedance measurement.

3.4. SEM images

In SEM images taken for sample P_6 after electrical measurement up to 550 °C (Fig. 7a) one can see nanocrystallites with a relatively uniform size below 100 nm. The shells seem to be strongly disordered and contacts between the grains are good. The microstructure of the active material for electrochemical measurements is quite similar to the previous one, consisting of nanograins with good contact through the grain boundaries. Some interesting nanorod-like grains were observed in several samples (Fig. 7b).

a) b)

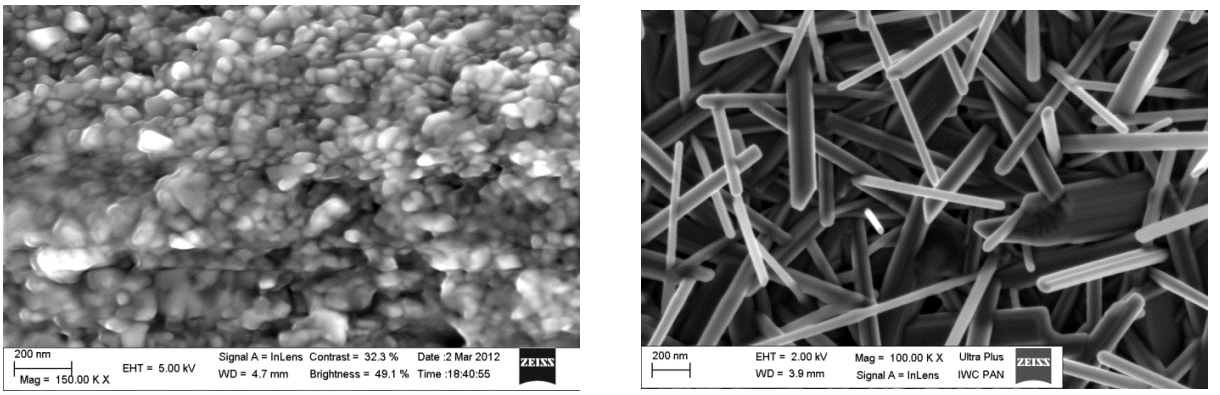

Fig. 7. SEM image of sample P_6: (a) after nanocrystallization at 550 °C during impedance measurements; (b) after nanocrystallization at 500 °C.

3.5. Electrochemical properties

The gravimetric capacity of the first discharge cycle at a C/20 current was 225 mAh/g and it dropped to 140 mAh/g after three cycles. The gravimetric capacity for C/10 current was ca. 90 mAh/g. However, the reversibility of the process for C/20 and C/10 was very good. A full discharge cycle (Fig. 8) showed that the maximum theoretical gravimetric capacity (398 mAh/g) can be reached for C/20 current. However, this caused a high voltage drop down to 0.4 V. Several smooth steps are observed on the discharge curve. This is characteristic for V_2O_5 crystallographic phase transitions reported for V_2O_5 upon intercalation [1, 21].

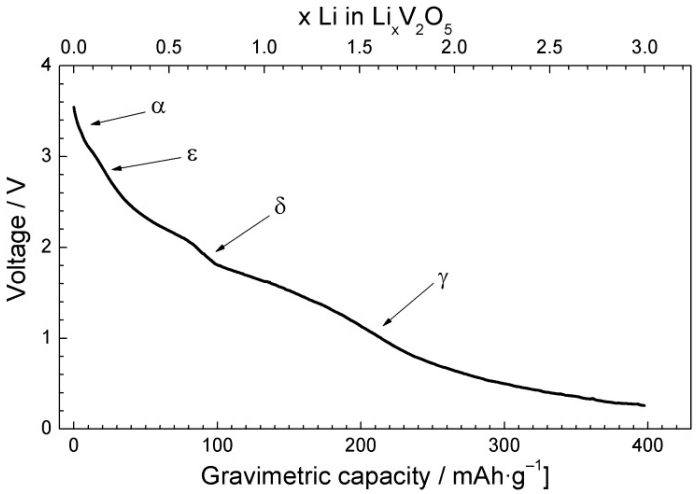

Fig. 8. Discharge curve with C/20 current for a laboratory cell with nanocrystalline sample as a cathode. V_2O_5 phase transitions are observable. Phases were ascribed on the bases of [1] and [21].

4. Discussion

It has been known that the annealing of batches of molten V_2O_5 at high temperatures leads to oxygen losses [22]. This is accompanied by reduction of a fraction of V^{5+} to V^{4+} ions and therefore has a positive impact on concentration of V^{4+}/V^{5+} hopping centers. One may therefore expect that higher temperature of melting will result in larger concentration of hopping centers. The expression for electronic conductivity in glasses containing transition metal oxides (in particular: vanadium) was given by Mott [20, 23]:

$$\sigma = \nu_{el} c(1-c) \frac{e^2}{R k_B T} \cdot \exp(-2\alpha R) \exp\left(-\frac{E_a}{k_B T}\right) \tag{3}$$

where R is the average distance between hopping centers, $\nu_{el} \approx \hbar/mR^2$, α is the inverse localization length of the electron wave function, $c = [V^{4+}]/([V^{4+}]+[V^{5+}])$ is the fraction of occupied hopping sites for electrons and E_a is the activation energy of electronic conduction. Assuming that all the pre-exponential factors are constant, one obtains Arrhenius formula.

The values of the electronic conductivity and temperatures of the glass transition and crystallization for bathes synthesized at various temperatures are in a good agreement with our predictions and previous studies. The increase in the temperature of the synthesis led to increase in concentration of V^{4+} ions. This causes greater value of $c(1–c)$ and smaller value of R term in Eq. 3 and consequently results in higher electronic conductivity and lower activation energy. Detailed discussion on this phenomenon can be found in [8]. The influence of a presence of aliovalent ions on DTA signals was studied by Doupovec et al. for iron glasses [24]. The authors showed that higher concentrations of Fe^{2+} ions resulted in higher T_c temperatures and a presence of second crystallization peak (in case of $[Fe^{2+}] > [Fe^{3+}]$). In our case, the shift towards higher temperatures is observed for both T_g and T_c, but no separation of the main crystallization peak can be observed. This can be explained assuming that the concentration of V^{5+} ions is still greater then V^{4+} ions. The activation energies of thermal transitions in the samples are quite similar for all the batches (i.e. ca. 7 eV for the glass transition and ca. 3 eV for the crystallization), but for P_6 they are noticeably lower, i.e. 4.7 eV and 2.2 eV, respectively. This may be correlated with better performance of nanocrystalline samples of batch P_6. The out-siding values for batch P_2 are apparatus artefacts rather than physical phenomenon.

The influence of the nanocrystallization on the electronic conductivity in vanadate-phosphate glasses has been discussed by us previously [8, 12, 25]. We have shown that Eq. 3 proposed by Mott for glassy materials, can be also

applied to nanomaterials obtained by nanocrystallization of these glasses. In our model, the concentration of hopping pairs (i.e. V^{4+}/V^{5+}) is greater in highly disordered surfaces of nanograins. Therefore, tightly packed small grains with high volume fraction of surface areas that are in good contact – i.e. giving conditions for fast electronic transport – result in high electronic (i.e. hopping) conductivity. Previously we studied nanocrystallization in $90V_2O_5 \cdot 10P_2O_5$ glasses synthesized only at one fixed temperature (950 °C). This approach resulted in a sample with conductivity of $2 \cdot 10^{-3}$ S/cm. In this paper, further optimization of the nanocrystallization process also included various temperatures of synthesis. As we had expected, higher temperature of synthesis (which resulted in higher concentration of V^{4+} hopping centers) led to higher conductivity enhancement after nanocrystallization up to 0.07 S/cm at RT. The greatest increase in the conductivity is correlated with second crystallization peak (Fig. 6) in batch P_6. However, for other batches, lower enhancement of the conductivity after annealing was observed (Fig. 5).

XRD and SEM measurements confirmed that high-conducting samples consist of V_2O_5 nanocrystallites. The larger mean grain size observed by SEM that by XRD can be explained in terms of a core-shell model [8, 12]. In this concept grains consist of crystalline core (observed by XRD) covered by disordered shell (discernible in SEM images). This issue was discussed in more detail e.g. in [8]. The presence of structures that resemble nanorods in some of the samples is not surprising, as V_2O_5 exhibit readiness to crystallize in a wide variety of nanostructures, e.g. nanotubes – VONTs [1], nanobelts [29], nanorods [30], or even nanoflowers [31]. It would be interesting to specify conditions under which a chance to produce such nanorods is high, but it was out of the scope of this research. It will be studied in a near future.

The main goal of this research was to better understand nanocrystallization process in vanadate glasses and to obtain high-conductive material rather than focus on optimizing electrochemical performance of laboratory cells. Nonetheless preliminary electrochemical measurements have shown that the material exhibit readiness to work as a cathode for lithium-ion batteries and lithium ions can be entirely intercalated into V_2O_5 microstructure. The advantage of obtained nanomaterial is that voltage drops corresponding to phase transitions of vanadium pentoxide, which are distinct for crystalline V_2O_5 [1, 21], in this case are smooth (Fig. 8).

5. Conclusions

- The temperature and the time of annealing melted substrates have significantly influenced the electronic conductivity, temperatures of the glass transition (T_g) and crystallization (T_c) of glassy samples. Higher temperature of the synthesis leads to a better electronic conductivity in glass and higher T_g and T_c.

- Thermal events taking place in glassy samples upon heating were shifted towards higher temperatures for larger heating rates. This behavior was satisfactorily described by Kissinger's formula. In case of the glass transition temperature, fitting with Lasocka's formula gave also good results.

- A significant increase in the electronic conductivity upon heating was observed for all the samples. This phenomenon was correlated with crystallization processes taking place in glassy samples. The heating of the samples led to a significant decrease in the activation energy of the electronic conductivity.

- The high electronic conductivity σ(25 °C) = 0.07 S/cm and low activation energy E_a = 0.13 eV were observed for a sample synthesized at 1300°C and nanocrystallized at 550 °C.

- XRD measurements and SEM images revealed the microstructure of the samples which consists of nanocrystallites with sub-100-nm size. The average size of nanograins in the sample selected for electrochemical measurements was 21 nm. In some samples structures similar to nanorods were observed.

- Preliminary electrochemical measurements showed good capability of a high conducting sample to intercalate 3 Li^+ ions per one V_2O_5. The gravimetric capacity for 1.5÷4.0 V range was moderate and equal to ca. 225 mAh/g for C/20 current. This is probably due to high loading of the cathode layer and in all likelihood can be optimized.

- Deep understanding of nanocrystallization processes in vanadate glasses is a good starting point to apply this technique to other systems (e.g. $LiFePO_4$ with addition of V_2O_5 [4, 32]) in order to obtain high-conductive cathode materials for lithium-ion batteries.

Acknowledgements

We are thankful to Prof. Jan L. Nowiński for assistance during XRD measurements and to Dr. Aldona Zalewska (Faculty of Chemistry, Warsaw University of Technology) for a helpful hand in electrochemical measurements.

References

[1] N.A. Chernova, M. Roppolo, A.C. Dillon, M.S. Whittingham, Journal of Materials Chemistry 19 (2009) 2526–2552.
[2] J. Hong, C.S. Wang, X. Chen, S. Upreti, M.S. Whittingham, Electrochemical and Solid-State Letters 12 (2009) A33–A38.
[3] F. Omenya, N.A. Chernova, S. Upreti, P.Y. Zavalij, K.-W. Nam, X.-Q. Yang, M.S. Whittingham, Chemistry of Materials 23 (2011) 4733–4740.
[4]T.K. Pietrzak, M. Wasiucionek, I. Gorzkowska, J.L. Nowiński, J.E. Garbarczyk, Solid State Ionics 251 (2013) 40-46 .
[5] R. Malik, D. Burch, M. Bazant, G. Ceder, Nano Letters 10 (2010) 4123–4127.
[6] S.-L. Chou, J.-Z. Wang, J.-Z. Sun, D. Wexler, M. Forsyth, H.-K. Liu, D.R. MacFarlane, S.-X. Dou, Chemistry of Materials 20 (2008) 7044–7051.
[7] L. Murawski, C. Sanchez, J. Livage, J.P. Audiere, Journal of Non-Crystalline Solids 124(1990) 71–75.
[8] T.K. Pietrzak, J.E. Garbarczyk, I. Gorzkowska, M. Wasiucionek, J.L. Nowiński, S. Gierlotka, P. Jóźwiak, Journal of Power Sources 194 (2009) 73–80.
[9] J.E. Garbarczyk, P. Jóźwiak, M. Wasiucionek, J.L. Nowiński, Solid State Ionics 175 (2004) 691–694.
[10] J.E. Garbarczyk, P. Jóźwiak, M. Wasiucionek, J.L. Nowiński, Journal of Power Sources 173 (2007) 743–747.
[11] J.E. Garbarczyk, P. Jóźwiak, M. Wasiucionek, J.L. Nowiński, Solid State Ionics 177 (2006) 2585–2588.
[12] T.K. Pietrzak, J.E. Garbarczyk, M. Wasiucionek, I. Gorzkowska, J.L. Nowiński, S. Gierlotka, Solid State Ionics 192 (2011) 210–214.
[13] T.K. Pietrzak, M. Maciaszek, J.L. Nowiński, W. Ślubowska, S. Ferrari, P. Mustarelli, M. Wasiucionek, M. Wzorek, J.E. Garbarczyk, Solid State Ionics 225 (2012) 658–662.
[14] A.L. Patterson, Physical Review 56 (1939) 978-982.
[15] T.K. Pietrzak, Ł. Wewiór, J.E. Garbarczyk, M. Wasiucionek, I. Gorzkowska, J.L. Nowiński, S. Gierlotka, Solid State Ionics 188 (2011) 99–103.
[16] R. Vaish, K.B.R. Varma, Journal of Physics D: Applied Physics 42 (2009) 015409.
[17] M. Lasocka, Materials Science and Engineering 23 (1976) 173–177.
[18] H.E. Kissinger, Analytical Chemistry 29 (1957) 1702–1706.
[19] J. Vázquez, C. Wagner, P. Villares, R. Jimenez-Garay, Journal of Non-Crystalline Solids 235–237 (1998) 548–553.
[20] I. G. Austin, N. F. Mott, Advances in Physics 18 (1969) 41–102.
[21] C. Delmas, H. Cognac-Auradou, J.M. Cocciantelli, M. Ménétrier, J.P. Doumerc, Solid State Ionics 69 (1994) 257–264.
[22] T. Szörenyi, K. Bali, I. Hevesi, Physics and Chemistry of Glasses 23 (1982) 42–44.
[23] N.F. Mott, Advances in Physics 16 (1967) 49–144.
[24] J. Doupovec, J. Sitek, J. Kákoš, Journal of Thermal Analysis 22 (1981) 213-219.
[25] T.K. Pietrzak, M. Wasiucionek, J.L. Nowiński, J.E. Garbarczyk, Solid State Ionics 251 (2013) 78-82.
[26] N. Ravet, A. Abouimrane, M. Armand, Nature Materials 2 (2003) 702–703.
[27] P. Subramanya Herle, B. Ellis, N. Coombs, L.F. Nazar, Nature Materials 3 (2004) 147–152.
[28] A. Ait Salah, A. Mauger, C.M. Julien, F. Gendron, Materials Science and Engineering B 129 (2006) 232–244.
[29] Y. Wang, G. Cao, Advanced Materials 20 (2008) 2251–2269.
[30] A.M. Glushenkov, V.I. Stukachev, M.F. Hassan, G.G. Kuvshinov, H.K. Liu, Y. Chen, Crystal Growth & Design 8 (2008) 3661–3665.
[31] M.R. Parida, C. Vijayan, C.S. Rout, C.S.S. Sandeep, R. Philip, P.C. Deshmukh, Journal of Physical Chemistry C 115 (2011) 112–117.
[32] T.K. Pietrzak, I. Gorzkowska, J.L. Nowiński, J.E. Garbarczyk, M. Wasiucionek, Functional Materials Letters 4 (2011) 143–145.